Solution Structure and Backbone Dynamics of the K18G/R82E *Alicyclobacillus acidocaldarius* Thioredoxin Mutant: A Molecular Analysis of Its Reduced Thermal Stability[†,‡]

Marilisa Leone,[§] Paola Di Lello,[#] Oliver Ohlenschläger,[||] Emilia M. Pedone,[§,⊥] Simonetta Bartolucci,[⊥] Mosè Rossi,[⊥] Benedetto Di Blasio,[#] Carlo Pedone,[§,⊥] Michele Saviano,[§,⊥] Carla Isernia,[#] and Roberto Fattorusso*[,#]

Istituto di Biostrutture e Bioimmagini, Via Mezzocannone 6/8, 80134 Napoli, Italy, Dipartimento di Scienze Ambientali, Seconda Università di Napoli, via Vivaldi 43, 81100 Caserta, Italy, Institut für Molekulare Biotechnologie, Beutenbergstrasse 11, D-07745, Jena, Germany, and Dipartimento di Chimica Biologica, Università di Napoli "Federico II", Via Mezzocannone 16, 80134, Napoli, Italy

Received December 17, 2003; Revised Manuscript Received February 27, 2004

ABSTRACT: No general strategy for thermostability has been yet established, because the extra stability of thermophiles appears to be the sum of different cumulative stabilizing interactions. In addition, the increase of conformational rigidity observed in many thermophilic proteins, which in some cases disappears when mesophilic and thermophilic proteins are compared at their respective physiological temperatures, suggests that evolutionary adaptation tends to maintain corresponding states with respect to conformational flexibility. In this study, we accomplished a structural analysis of the K18G/R82E *Alicyclobacillus acidocaldarius* thioredoxin (BacTrx) mutant, which has reduced heat resistance with respect to the thermostable wild-type. Furthermore, we have also achieved a detailed study, carried out at 25, 45, and 65 °C, of the backbone dynamics of both the BacTrx and its K18G/R82E mutant. Our findings clearly indicate that the insertion of the two mutations causes a loss of energetically favorable long-range interactions and renders the secondary structure elements of the double mutants more similar to those of the mesophilic *Escherichia coli* thioredoxin. Moreover, protein dynamics analysis shows that at room temperature the BacTrx, as well as the double mutant, are globally as rigid as the mesophilic thioredoxins; differently, at 65 °C, which is in the optimal growth temperature range of *A. acidocaldarius*, the wild-type retains its rigidity while the double mutant is characterized by a large increase of the amplitude of the internal motions. Finally, our research interestingly shows that fast motions on the pico- to nanosecond time scale are not detrimental to protein stability and provide an entropic stabilization of the native state. This study further confirms that protein thermostability is reached through diverse stabilizing interactions, which have the key role to maintain the structural folding stable and functional at the working temperature.

Proteins exhibit modest stabilities, which are equivalent to a small number of weak interactions (*1*, *2*). Indeed, in most globular proteins, the factors that favor formation of the native state, primarily desolvation of hydrophobic groups and ionic interactions, are almost equally balanced against those that favor denaturation, primarily the higher conformational entropy of the unfolded protein chain relative to that of the native state (*3*, *4*). In this respect, proteins from thermophilic organisms do not differ strongly from their mesophilic counterpart. Their adaptation, either intrinsic or through interaction with an extrinsic factor, is accompanied by only marginal increases in the free energy of stabilization. No general strategy for thermostability has been yet established (*5*), because the extra stability of thermophiles appears to be the result of different cumulative stabilizing interactions. Among them, the packing efficiency (mainly through van der Waals' interactions), networks of ion pairs and/or hydrogen bonds (including α-helix stabilization), the reduction of conformational strain (loop stabilization), and resistance to chemical modifications very often have been found to be responsible for protein thermal stabilization (*2*, *5*). In addition, the increase of conformational rigidity observed in many thermophilic proteins, which in some cases disappears when mesophilic and thermophilic proteins are compared at their respective physiological temperatures (*6*), suggests that evolutionary adaptation tends to maintain corresponding states with respect to conformational flexibility, that way optimizing biological function under specific physiological conditions (*7*). Thus, structural analyses of thermostable proteins combined with investigations of their dynamic behavior at different temperatures constitute an important step to identify structural and dynamic determi-

[†] This work was supported by the European Commission under Contract No. ERB-FMGE-CT98-0121/HPRI-CT-1999-00097 (C.I. and R.F.) and by a PRIN 2002 grant from Ministero dell'Istruzione, dell'Università e della Ricerca (S.B., E.M.P., and M.R.).

[‡] PDB entry: 1RQM. BMRB accession codes: 5240 (BacTrx ^{15}N assignments) and 5241 (K18G/R82E BacTrx ^{1}H and ^{15}N assignments).

* Corresponding author footnote: Telephone: +39 0823 274637. Fax: +39 0823 274605. E-mail: roberto.fattorusso@unina2.it.

[§] Istituto di Biostrutture e Bioimmagini.

[#] Seconda Università di Napoli.

[||] Institut für Molekulare Biotechnologie.

[⊥] Università di Napoli "Federico II".

10.1021/bi036261d CCC: $27.50
Published on Web 04/29/2004

nants at the bases of their stability and functionality at higher temperatures.

Thioredoxins belong to a family of proteins present in all living cells from *Archaea* to humans. These proteins are involved in several fundamental cellular processes such as regulation of transcription factors, activation of deoxyribonucleotides biosynthesis, regeneration of oxidative damage, and regulation of photosynthetic events (*8*). This class of proteins is structurally well characterized by NMR and X-ray techniques (*9*−*17*), and backbone dynamics studies have already been reported for *Escherichia coli* thioredoxin (*18*), for the thioredoxin from green alga (*15*), and for the human−*E. coli* thioredoxin chimera (*17*).

Thioredoxin (Trx)[1] is a small globular protein (10−12 kDa) that is highly structured with 90% of its residues involved in secondary structure elements (*19*). The tertiary fold of Trx consists of a central core of a five-stranded β-sheet surrounded by four exposed α-helices. The active site, containing two cysteine residues in a highly conserved sequence (**Cys**-Gly-Pro-**Cys**), is located in a small loop of the molecule at the N-terminal region of the second helix. A novel thioredoxin (105 a.a.) was isolated from the moderate thermophile *Alicyclobacillus acidocaldarius* (first denominated *Bacillus acidocaldarius*) in 1997, and its sequence as well as the physicochemical properties were described (*20*). Structural stability studies carried out on *A. acidocaldarius* thioredoxin (BacTrx) by means of circular dichroism, differential scanning calorimetry, and nanogravimetry showed that BacTrx withstands higher temperatures than the thioredoxin from the mesophilic bacterium *E. coli* despite their high sequence identity (49%). Molecular dynamics simulation studies performed in vacuo and in aqueous solution at different temperatures allowed the derivation of structural information on the determinants of thermal stability of BacTrx and permitted the design of mutants with reduced heat capacity (*21*). The residues Lys18 and Arg82 of BacTrx, which appeared to be involved in stabilizing interactions, such as hydrogen bonds and ion-pairs, were replaced by means of site-directed mutagenesis with Gly and Glu, respectively, which are present in the corresponding positions of the *E. coli* thioredoxin. The effects of the point mutations on the protein thermal stability were monitored by CD spectroscopy, spectrofluorimetry, and thermodynamic comparative studies, and the mutants were shown to be substantially less stable ($\Delta T_m < 12-15°$) when compared to the wild-type (*22*, *23*). Among all the proteins produced, the K18G/R82E BacTrx mutant showed the most significant differences. In 2000, the solution structure of BacTrx was reported (*14*); the structure, derived on the basis of homonuclear NMR data, retains the typical thioredoxin fold. The solution structure confirms the validity of the model used to obtain the structural information concerning the determinants of thermal stability in BacTrx (*21*).

In this paper, we report the high-resolution NMR structure determination of the K18G/R82E BacTrx mutant and its comparison with the wild-type protein. In addition, we also present a detailed study, accomplished at different temperatures, of the backbone dynamics of both the BacTrx and its K18G/R82E mutant. The comparison of either structure and backbone dynamics of the wild-type and mutant thioredoxins provides important insights into molecular interactions at the basis of protein thermal stability.

MATERIALS AND METHODS

Protein Expression, Purification, and NMR Sample Preparation. To obtain ^{15}N labeled proteins, *E. coli* strain JM101 was grown on M9 minimal medium containing 1 g/L of $^{15}NH_4Cl$, and the whole extract was hydrolyzed to free labeled amino acids. *E. coli* strain Rb791, transformed with a recombinant pTrc99A plasmid carrying the gene coding for the wild-type protein and for the K18G/R82E double mutant, was grown in minimal medium containing the ^{15}N labeled hydrolyzed. The optimized overexpression of both the proteins was reached by exposing the cells to 1 mM isopropyl β-D-thiogalactoside (IPTG) at a cell density of $OD_{600\ nm} = 1$ for 20 h. For NMR experiments, both proteins were dissolved at a concentration of 0.5 mM in 90%H_2O−10%^2H_2O or in pure ^2H_2O, 100 mM potassium phosphate pH 6.0.

NMR Measurements. NMR spectra were collected on Varian ^{UNITY}*INOVA* 750 and 600 MHz spectrometers equipped with a 5-mm triple resonance probe and *z*-axis pulsed-field gradients, located at the Centre for Design and Structure in Biology (CDSB), Jena, Germany. 3D spectra ^{15}N-edited TOCSY−HSQC (*24*), ^{15}N-edited NOESY−HSQC (*25*), HNHA (*26*), and HNHB (*27*) and 2D [^1H,^{15}N] HSQC (*28*) were recorded on a ^{15}N-labeled sample dissolved in 90% H_2O−10% ^2H_2O; 2D TOCSY (*29*), NOESY (*30*) and double quantum-filtered COSY (*31*) experiments were carried out with a sample in pure ^2H_2O.

[^1H,^{15}N] HSQC spectra were recorded at 25, 35, 45, 55, and 65 °C, with 2048 (H^N) and 128 (^{15}N) real data points acquired with a total of 8 transients per t_1 increment. 3D^{15}N-edited TOCSY−HSQC (45 ms mixing time), ^{15}N-edited NOESY−HSQC (70 ms mixing time), HNHA, HNHB were recorded at 25 °C with 2048 (H^N), 96 (H), 32 (^{15}N) real data points acquired with a total of four transients per increment. The spectral widths for $^1H^N$, ^1H, and ^{15}N were 10 000, 8000, and 2500 Hz, respectively. TOCSY transfer was achieved using a DIPSI isotropic mixing sequence (*32*). All the experiments were performed using gradient sensitivity enhancement (*33*), and ^{15}N decoupling was performed during acquisition using a 1.25 kHz GARP sequence.

2D-TOCSY experiments were recorded using a MLEV17 mixing scheme of 70 ms (spectral width 10 000 Hz both along f_1 and f_2, 2048 × 256 data points in t_2 and t_1 respectively, recycle delay 3 s, 16 scans per t_1 increment). The 2D NOESY spectrum was carried out by the standard pulse sequence with a mixing time of 70 ms (spectral width 10 000 Hz along both f_1 and f_2, 4096 × 512 data points in t_2 and t_1 respectively, recycle delay 3 s, and 72 scans per t_1

[1] Abbreviations: BacTrx, *Alicyclobacillus acidocaldarius* thioredoxin; CD, circular dichroism; COSY, correlated spectroscopy; CPMG, Carr-Purcell-Meiboom-Gill; CYANA, combined assignment and dynamics algorithm for NMR applications; DIPSI, decoupling in the presence of scalar interactions; EcTrx, *Escherichia coli* thioredoxin; HSQC, heteronuclear single quantum coherence; IPTG, isopropyl β-D-thiogalactopyranoside; MLEV, Malcolm Levitt; NMR, nuclear magnetic resonance; NOE, nuclear Overhauser effect; NOESY, nuclear Overhauser effect spectroscopy; PFG, pulsed field gradient; R_1, longitudinal relaxation rate constant; R_2, transversal relaxation rate constant; rmsd, root-mean-square deviation; SD, standard deviation; TOCSY, total correlation spectroscopy; TPPI, time proportional phase incrementation; Trx, thioredoxin.

increment). The 2D DQF−COSY was obtained in the TPPI phase sensitive mode (spectral width 10 000 Hz along both f_1 and f_2, 4096 × 768 data points in t_2 and t_1, respectively, recycle delay 2.5 s, and 96 scans per t_1 increment).

Water suppression was achieved by means of solvent presaturation during the recycle delay (2.5 s) for samples in ^2H_2O solution or by means of the WATERGATE PFG technique in the case of $H_2O/^2H_2O$ solution.

To determine the degree of solvent exposition of the amide protons, a series of HSQC was recorded using a sample dissolved in pure ^2H_2O. HN groups, whose resonances were observed after 24 h the protein was dissolved in ^2H_2O, were assumed to have low solvent exposition and possible implication in hydrogen-bond formation.

Proton chemical shifts were referenced to the water signal (4.75 ppm); an external standard (NH_4Cl) was used for referencing the nitrogen chemical shift.

NMR spectra were processed using the VNMR 6.1B software (Varian, Palo Alto) and were analyzed with the program XEASY (*34*).

^{15}N Backbone Relaxation Measurements. ^{15}N relaxation parameters (longitudinal relaxation rates (R_1), transversal relaxation rates (R_2), and heteronuclear ^{15}N-{^1H}-NOE) were measured for BacTrx mutant and wild-type at 25, 45, and 65 °C on a Varian ^{UNITY}*INOVA* 600 MHz spectrometer located at the 'Istituto di Biostrutture e Bioimmagini' CNR, Naples, Italy. For relaxation experiments, both proteins were dissolved at a concentration of 0.5 mM in 90%H_2O−10%^2H_2O, 100 mM potassium phosphate, pH 6.0.

Gradient-enhanced pulse sequences were used to minimize water saturation (*35*). R_1 and R_2 relaxation data were collected as 2048 (t_2) per 150 (t_1) complex points, with 16 transients; NOE experiments were recorded as 575 (t_2) per 256 (t_1) real data points, with 16 transients per increment. The ^1H and ^{15}N spectral widths were 10 and 2.8 kHz, respectively.

Six experiments were performed for R_1 measurements, using different values of the relaxation delay (0.01, 0.1, 0.3, 0.6, 1.0, 1.3 s); R_2 data sets were obtained employing the following relaxation delays: 0.01, 0.3, 0.5, 0.7, 0.11, 0.15, 0.19 s.

In the R_2 pulse scheme, the relaxation delay was made up of 650 μs intervals flanking the ^{15}N 180° refocusing pulses. The recycle delay between transients was set to 1.8 s in the pulse sequences for R_1 and R_2 measurements.

The absence of aggregation processes which could raise R_2 values was checked by concentration-dependent measurement of R_2 (*36*).

For R_1 and R_2 duplicate experiments at all the time points were carried out to allow estimation of peak height uncertainties.

Two identical pairs of ^{15}N-{^1H}-NOE experiments were recorded at each temperature. In one experiment of each pair, proton were saturated for 3 s during the 5 s recycle delay (field strength 10 kHz); in the other experiment, a 5 s recycle delay was used without proton saturation. The uncertainty in the NOE values was set to 5% of their values (*37*, *38*).

Relaxation Data Processing and Analysis. The data for the measurement of relaxation parameters were Fourier transformed after application of a cosine-squared apodization function to yield a matrix of 2048 × 512 data points.

Peak intensities were measured rather than peak volume for the calculation of the relaxation times and heteronuclear ^{15}N-{^1H}-NOE values. R_1 and R_2 rates were determined by fitting the peaks heights at multiple relaxation delays to the equation $I = I_0e^{-(Rt)}$ (*38*) using MATLAB. Uncertainties in R_2 and R_1 were the obtained from the fit error. {^{15}N,^1H} steady-state NOEs were calculated as the ratio of ^1H-^{15}N correlation peak heights in the spectra acquired with and without three seconds of proton saturation during the five seconds recycle delay.

Estimation of the Molecular Diffusion Tensor. An initial estimate of the magnitude and orientation of the diffusion tensor at each temperature was obtained from the ratios of ^{15}N R_2 and R_1 values using the programs QUADRIC_DIFFUSION (*39*, *40*) and R_2R_1_1.1 (*41*). The fitting procedure was described by Tjandra et al. (1995). Residues with large amplitude fast internal motions were excluded from the calculation. Among the remaining residues, those with significant conformational exchange on the microsecond−millisecond time scale were also excluded.

Calculation of ModelFree Dynamics Parameters. The parameters R_1, R_2, and NOE are dependent on the spectral densities $J(\omega)$ at five frequencies (*42*). The R_2 may also include an additional contribution (R_{ex}) to account for chemical exchange processes which supplies to the decay of transverse relaxation during the CPMG pulse train or during the spin-locking period in the experiments used to measure R_2 (*43*). Relaxation data were fit to the ModelFree formalism using the following spectral density function for axially symmetric diffusion of molecule (*44*):

$$J(\omega) = (2/5)S^2{}_1\Sigma_{(j=1\ldots3)}A_j\{S^2{}_2[\tau_m/(1+(\omega\tau_m)^2)] + (1-S^2{}_2)[\tau_j'/1+(\omega\tau_j')^2]\}$$

where τ_m is the overall correlation time of the molecule; $\tau_j' = [(\tau_j\tau_e)/(\tau_j+\tau_e)]$, τ_e is the effective internal correlation time; $S^2 = S^2{}_1S^2{}_2$ is the square of the generalized order parameters describing the amplitude of internal motions; $\tau_1{}^{-1} = 6D_\perp$; $\tau_2{}^{-1} = 5D_\perp + D_\parallel$; $\tau_3{}^{-1} = 2D_\perp + 4D_\parallel$, $D_\parallel$ and $D_\perp$ are the diffusion constants for rotation around the unique and perpendicular axes, respectively; $A_1 = (3\cos^2\theta - 1)^2/4$; $A_2 = 3\sin^2\theta\cos^2\theta$; $A_3 = (3/4)\sin^4\theta$, where θ is the angle between the NH bond vector and the unique axis of the principal frame of the diffusion tensor.

The appropriate models for internal dynamics parameters were chosen using an iterative fitting procedure and statistical significance tests (*45*). Five different models were tested to characterize the internal dynamics of the NH groups; each model included optimization of different microdynamic parameters (S_1^2, S_2^2, τ_e, R_{ex}). Model 1 (*42*, *46*) characterized the internal dynamics of NH bond whose motion is very fast (<20 ps); for this model only a single very fast internal motion is assumed, $S^2{}_2$ is optimized and defined as $S^2{}_f$ (i.e., the square of the order parameter for fast internal motions) while assuming $S^2{}_1 = 1$, $\tau_e = \tau_f = 0$, and $R_{ex} = 0$. Model 2 is analogue to model 1, $S^2{}_f$, and τ_e (redefined as τ_f) are now optimized and τ_f is assumed to be in a time scale between 20 and 500 ps. Model 3 and model 4 are equivalent to model 1 and model 2, respectively, but include the optimization of a chemical exchange term R_{ex} in addition to the other microdynamic parameters (*18*, *47*, *48*). Model 5 characterizes internal motions on two different time scales both faster than the overall correlation time, $S^2{}_1$ is now redefined as $S^2{}_f$ (the

square of the order parameters on a fast time scale, faster than 20 ps), S^2_2 is redefined as S^2_s (the square of the generalized order parameters for internal motions on a slow time scale assumed slower than 500 ps).

ModelFree calculations have been carried out using the program ModelFree 4.0 (*18*, *48*). Uncertainties in the dynamical parameters were determined using Monte Carlo simulations performed by the ModelFree program.

Structure Calculations and Analysis. Distance constraints for structure calculations were obtained from two nuclear Overhauser enhancement spectroscopy (NOESY) experiments recorded at a proton frequency of 750 MHz: a 3D [^{1}H,^{1}H,^{15}N] NOESY−HSQC spectrum (70 ms mixing time) acquired on a sample in $H_2O/^2H_2O$ (90:10), and a 2D [^{1}H,^{1}H] NOESY (70 ms mixing time) acquired on a sample dissolved in pure ^2H_2O. NOE cross-peaks were manually integrated with the program XEASY. The program CYANA (*49*) was used to convert NOE intensities into upper distance bounds according to an inverse sixth power peak volume-to-distance relationship for the backbone and an inverse fourth power function for the side-chains, to perform a systematic grid search analysis of the local conformation along the polypeptide backbone with the FOUND module (*78*) and to calculate structures with the torsion angle dynamics protocol. Finally, structure calculations were started from 100 randomized conformers. During the calculations, lower and upper limit distance constraints were used for the disulfide bridge between Cys29 and Cys32, in addition Pro73 was settled in a cis conformation. The 20 conformers with the lowest CYANA target function were further refined by means of restrained energy minimization, using the AMBER force field, with the program OPAL (*50*).

Structures were analyzed with the programs MOLMOL (*51*) and PROCHECK−NMR (*52*).

Structural features presented in Table 5 were calculated using the mean structures of the NMR ensemble of BacTrx (PDB code 1QUW) and its mutant; for EcTrx the mean structure of the two monomers in the crystal structure (PDB code 2TRX), was considered. The number of residues in β-sheet and α-helix and ion pairs were estimated with the program MOLMOL. The number of residues in β-sheet elements was estimated excluding the first β-strand, which is disordered in the BacTrx mutant structure.

Short- and long-range ion-pairs were evaluated using the criterion of a distance < 4 and < 7 Å, respectively, between the positively charged side-chain of Lys(NZ), Arg(NH1; NH2), and His(NE2) and the negatively charged side-chain of Glu(OE1; OE2) and Asp (OD1;OD2).

RESULTS

Resonance Assignments, Conformational Constraints, and Structure Calculations. After the identification of ^{15}N and H^N chemical shifts of the K18G/R82E BacTrx mutant in the [^{1}H,^{15}N] HSQC spectrum, the sequence-specific backbone assignment was obtained with the combined use of 3D ^{15}N-edited NOESY−HSQC, 3D ^{15}N-edited TOCSY−HSQC, HNHA, HNHB spectra. Full side-chain ^{1}H assignment was achieved after the analysis of 2D double quantum-filtered COSY, NOESY, and TOCSY spectra recorded on a sample in pure ^2H_2O. The ^{15}N assignments of the wild-type thioredoxin were obtained from 3D ^{15}N-edited TOCSY−HSQC, ^{15}N-edited NOESY−HSQC, and [^{1}H,^{15}N] HSQC spectra, using the proton assignments as previously published (*14*). Starting from ^{15}N and $^1H^N$ assignment at 25 °C, the assignments at higher temperature (45 and 65 °C) were obtained by the analysis of a series of [^{1}H,^{15}N] HSQC recorded every 5 °C in the temperature range 25−65 °C.

Table 1: Statistics for the Final 20 Structures of the K18G/R82E BacTrx Mutant

quantity	value
NOE upper distance limits	1546
dihedral angle constraints	505
residual target function, Å^2	1.32 ± 0.14
residual NOE violations	
no. > 0.2 Å	0.7 ± 0.7
maximum, Å	0.23 ± 0.06
residual angle violations	
no. > 5.0°	0 ± 0
maximum, °	0.07 ± 0.02
amber energies, kcal/mol	
total	−1538 ± 70
van der Waals	−323 ± 19
electrostatic	−2021 ± 85
RMSD[a], Å	
backbone[b] (1−105)	0.65
all heavy (1−105)	1.07
backbone β-sheet	0.33
backbone helices	0.52
backbone active site (26−32)	0.31
all heavy active site (26−32)	0.45

[a] rms deviation values are the average pairwise rms deviations for the residues and atoms specified, relative to the geometric average of the corresponding ensemble of 20 structures. [b] (N, C$^\alpha$, C′, O) were used for the superposition.

Conformational constraints for structure calculations were obtained from NOE upper distance limits and from scalar spin−spin couplings. Out of a total of 2052 cross-peaks assigned, 937 were derived from 3D ^{15}N-edited NOESY−HSQC and 1107 from 2D [^{1}H,^{1}H] NOESY acquired in pure ^2H_2O. Inverse Fourier transform of in-phase multiplets from a 2D [^{1}H,^{15}N] HSQC spectrum provided 64 $^3J_{HNH\alpha}$ coupling constants. Stereospecific assignments for six degenerate pairs of diastereotopic β-methylene protons and two valine γ-methyl groups were obtained using the HABAS module of CYANA (*53*).

The input for the final CYANA structure calculation contained 1546 upper limit distance constraints (358 intra, 374 short-range, 319 medium-range, 495 long-range, and 505 torsion angle constraints (Table 1)). Six additional constraints (three lower and three upper) were added for the disulfide bond between Cys29 and Cys32; the Pro73 was set in a cis configuration as it is indicated by the NOE pattern and as it was found in the wild-type and in the other mutant structures (*54*). A total of 100 structures were calculated with the program CYANA (*49*) and the 20 conformers with the lowest CYANA target functions were further refined by means of restrained energy minimizations with the program OPAL (*51*).

The small number of residual constraint violations (Table 1) indicates that the input data represents a self-consistent set and that the constraints are well satisfied in the calculated conformers. The global root-mean-square deviation (rmsd) values calculated for different residue selections (Table 1) show that the overall high precision of the structure determination has been achieved.

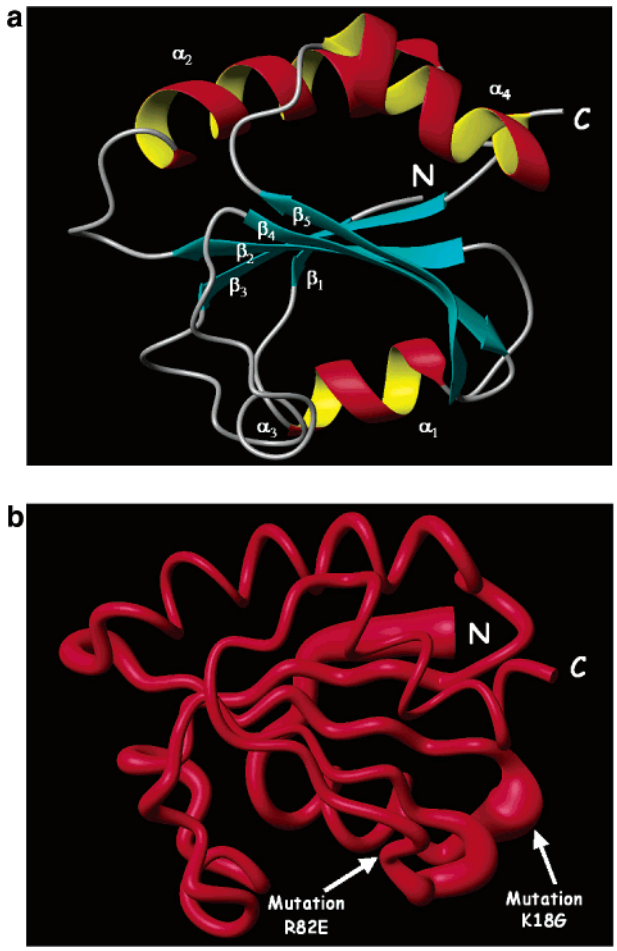

FIGURE 1: (a) The ribbon drawing of one representative conformer of the K18G/R82E BacTrx NMR structure. (b) Sausage representation of the K18G/R82E BacTrx NMR ensemble of structures. The regions around the two mutations are indicated by arrows.

The high quality of the final structures was also proven with the program PROCHECK−NMR (*52*), which indicated that 82.5% of the residues fall into the most favorite and 16.5% in the allowed or generously allowed regions of the Ramachandran map.

The NMR Structure of the K18G/R82E Alicyclobacillus acidocaldarius Thioredoxin. The ribbon drawing of a representative structure of the K18G/R82E BacTrx double mutant is shown in Figure 1a. It adopts the canonical thioredoxin fold (*55*) with α1-*β*1-*β*2-α2-*β*3-α3-*β*4-*β*5-α4 topology. Its tertiary structure consists of a central core of *β*-sheet made up of five strands which adopt the following orientation ↑↑↑↓↑ and are surrounded by four exposed helices. The C-terminal helix α4 is actually composed of two helical segments (93−99 and 101−104) with different orientation axes. On one side of the *β*-sheet the two helices α1 and α3 pack against each other running in a parallel manner; the α2 helix is located on the other side of the *β*-sheet, presenting perpendicular orientation with respect to α1 and α3. The active site loop, which ranges from Ala26 at the end of *β*2 to Cys32 at the beginning of the α2-helix and comprises the two Cys residues 29 and 32 with redox activity (*22*), is also very well defined (Table 1).

The backbone superposition of the 20 energy-minimized structures of K18G/R82E BacTrx is depicted in Figure 1b. The secondary structure elements are very well defined (Table 1), particularly the strands constituting the core *β*-sheet, with the exception of the more disordered *β*1-strand. As expected, the loop regions contain a higher structural disorder, in particular that between α1 and *β*2 (backbone $rmsd_{15-19}$ = 0.61 Å), where the mutation of residue 18 occurs, while the region between *β*4 and *β*5, in the proximity of the mutation 82, is better defined (backbone $rmsd_{79-83}$ = 0.26 Å).

Relaxation Parameters, Estimation of Correlation Time and Rotational Diffusion. The three relaxation parameters R_1, R_2, and ^{15}N-{^{1}H}-NOE have been measured for both BacTrx and the K18G/R82E mutant at temperatures of 25, 45, and 65 °C. Experimental values and uncertainties have been determined as described in Materials and Methods. Figure 2 shows the graphs of the relaxation parameters vs residue numbers. Relaxation parameters are generally constant along the secondary structure elements as expected for a rigid structure, whereas they are well below the mean values in the loop regions, mainly in the portion around the first mutation (residue 18) and at the C-terminus where also negative values of the NOE were found at the higher temperatures (Figure 2). Furthermore, R_2 values higher than the mean mainly occur for those residues encompassing the active site (26−32) or the loops around residues 70 and 90 which are located spatially close to the active site.

At 25 and 45 °C, the values of relaxations parameters for the wild-type and the mutant are rather similar within the experimental error (Table 2). At 65 °C, the NOE values for the K18G/R82E BacTrx mutant show a net decrease with respect to the wild-type, even if R_1 and R_2 average values remain rather similar.

In absence of conformational exchange and provided that the extreme narrowing condition for fast internal motions is satisfied, the R_2/R_1 ratio can be used to obtain an initial estimation of the overall molecular correlation time τ_m (*41*, *56*), with the exclusion of the residues exhibiting large amplitude internal motions (low NOE values) or possible conformational exchange (R_2/R_1 > 1.5 SD, where SD is the standard deviation from the average value). Seventy-four residues were used to calculate the mean R_2/R_1 ratio of the wild-type protein at 25 °C, yielding to a value of 4.9 ± 0.5. At 45 and 65 °C, 81 residues and 76 residues, respectively, were included in the calculation resulting in R_2/R_1 ratios of 2.5 ± 0.2 and 1.7 ± 0.3, respectively.

For the K18G/R82E BacTrx mutant, the mean R_2/R_1 ratio at 25 °C, calculated using 80 residues, was 5.1 ± 0.4. At 45 °C, a total of 83 spins were included in the calculation and the average R_2/R_1 ratios resulted 2.3 ± 0.2, while at 65 °C the mean R_2/R_1 ratio resulted in 1.6 ± 0.2, utilizing 69 residues in the analysis.

The initial estimations of τ_m (Table 3) were later optimized with the ModelFree protocol (*18*, *48*). As it is expected on the basis of the Stokes−Einstein relationship, τ_m values decrease with temperature, reflecting a reduction in solvent viscosity as a function of increased temperature. At 65 °C, the estimation of τ_m of the mutant protein has to be considered only tentative because the NOE low values indicate high internal mobility and the description of the molecular tumbling in terms of a single correlation time is unlike to correctly explain the motion of the mutant protein at this temperature.

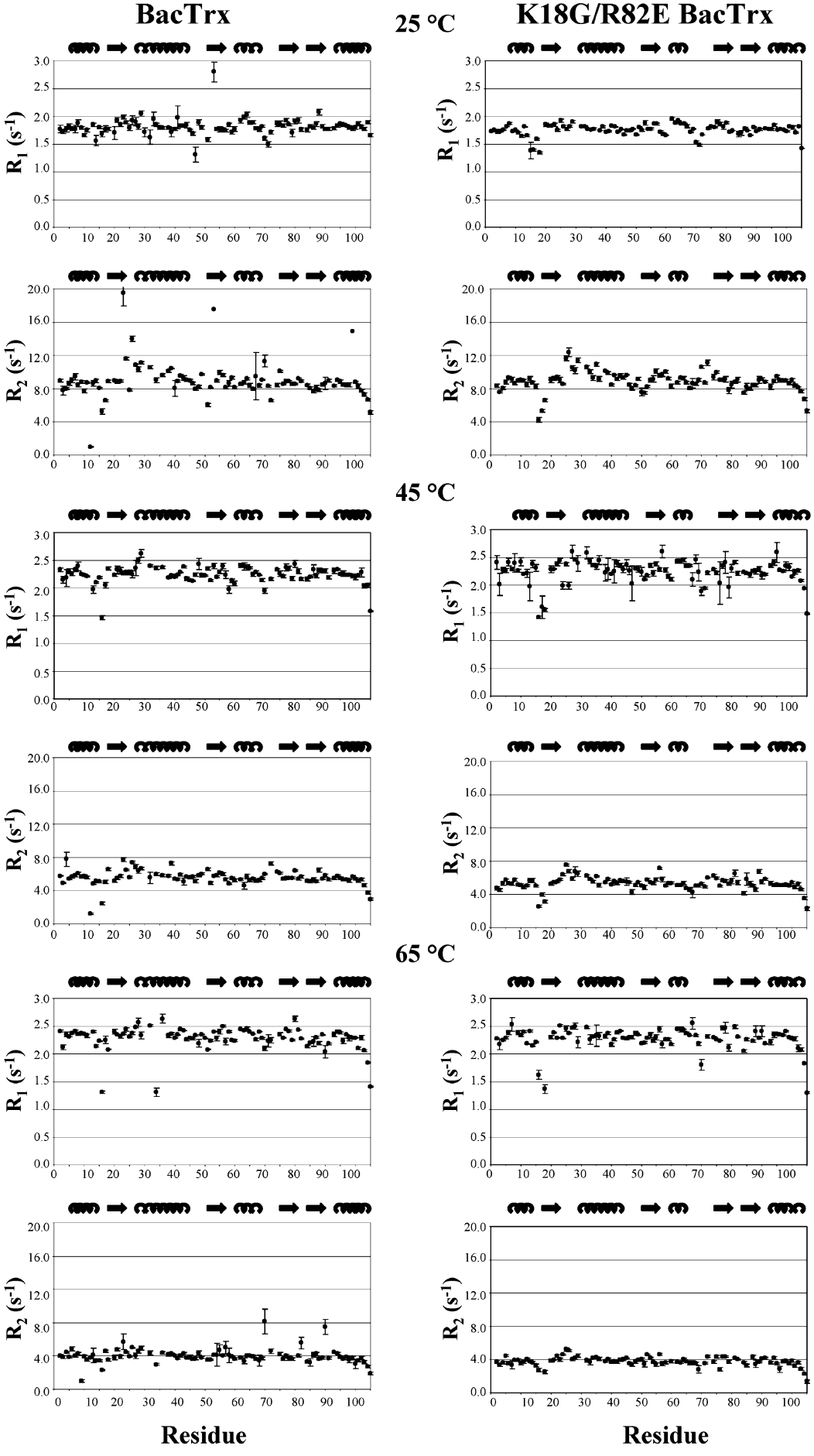
BacTrx
K18G/R82E BacTrx
25 °C
45 °C
65 °C
R1 (s-1)
R2 (s-1)
Residue
Residue

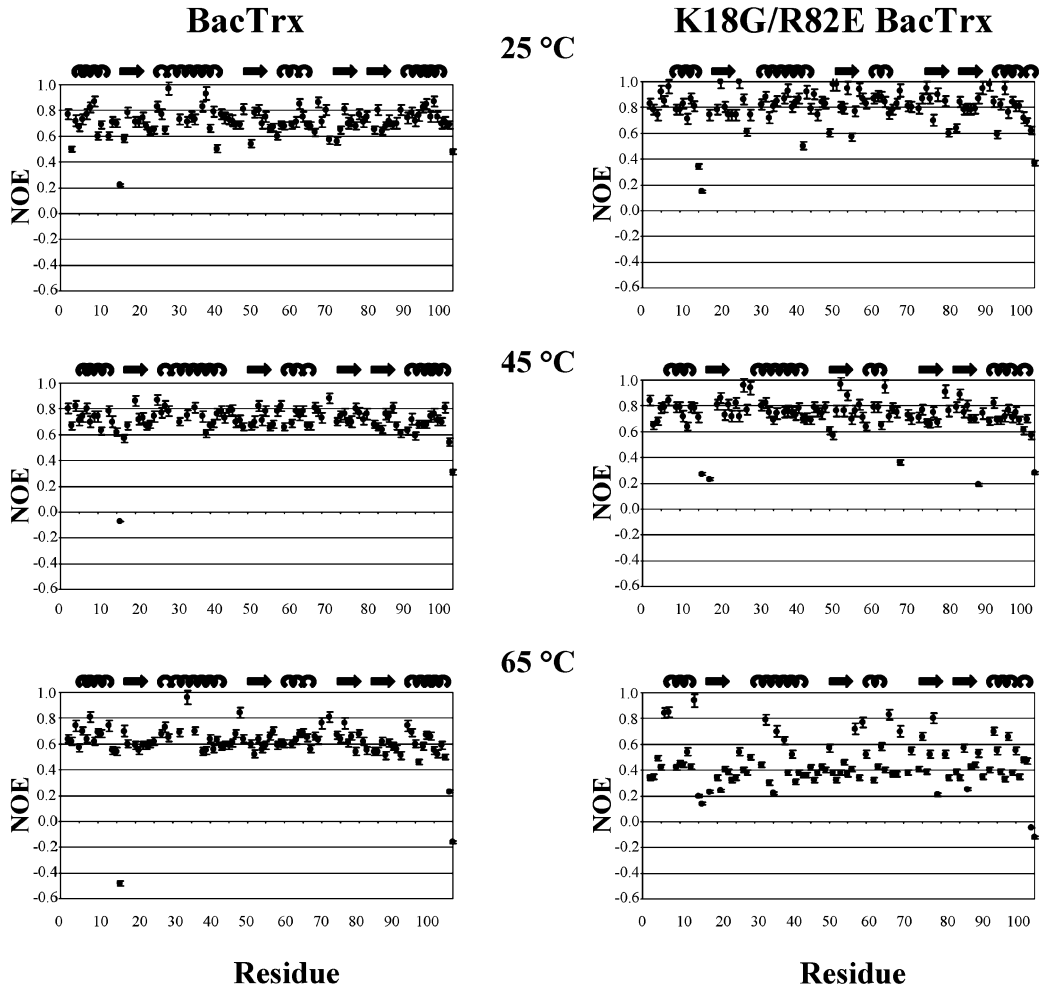

FIGURE 2: Relaxation parameters (R_1, R_2, and ^{15}N-{^{1}H}-NOE) of BacTrx and its K18G/R82E mutant plotted versus the residue numbers.

Table 2: Average Relaxation and Dynamical Parameters

BacTrx	25 °C	45 °C	65 °C
R_1	1.80 (0.09)[a]	2.3 (0.1)	2.3 (0.1)
R_2	8.7 (0.9)	5.6 (0.4)	3.9 (0.4)
NOE	0.72 (0.07)	0.74 (0.05)	0.62 (0.07)
S^2	0.88 (0.08)	0.86 (0.05)	0.82 (0.09)
cone semi-angle	16.6°	18.1°	20.7°
K18G/R82E BacTrx	**25 °C**	**45 °C**	**65 °C**
R_1	1.76 (0.06)	2.3 (0.1)	2.3 (0.1)
R_2	8.9 (0.8)	5.4 (0.5)	3.8 (0.4)
NOE	0.82 (0.06)	0.74 (0.05)	0.41(0.08)
S^2	0.88 (0.07)	0.83 (0.09)	
cone semi-angle	16.6°	20.0°	

[a] Numbers in parentheses are the standard deviations.

Table 3: Molecular Rotational Diffusion Parameters Obtained from the R_2/R_1 Ratios, Used as Input for the ModelFree Analysis

BacTrx	25 °C	45 °C	65 °C
$D_{II}/D_{\perp}$	1.186 ± 0.004	0.863 ± 0.007	0.80 ± 0.04
θ (deg)	0.46 ± 0.01	1.40 ± 0.04	0.17 ± 0.13
φ (deg)	2.05 ± 0.02	3.69 ± 0.03	3.1 ± 0.7
τ_m (ns)	6.3 ± 0.6	3.7 ± 0.3	2.4 ± 0.3
K18G/R82E BacTrx	**25 °C**	**45 °C**	**65 °C**
$D_{\|}/D_{\perp}$	1.126 ± 0.001	1.17 ± 0.01	0.76 ± 0.02
θ (deg)	0.682 ± 0.01	0.42 ± 0.04	1.09 ± 0.07
φ (deg)	5.15 ± 0.02	2.04 ± 0.09	3.78 ± 0.05
τ_m (ns)	6.4 ± 0.3	3.5 ± 0.3	2.3 ± 0.3

To estimate possible effects of anisotropic rotational diffusion, the principal moments of inertia tensor of the K18G/R82E mutant and the wild-type proteins were determined from the coordinates of the mean NMR structures using the software PDBINERTIA (*39*). The ratios of the principal moments were found to be (1.00, 0.77, 0.72) and (1.00, 0.78, 0.70) for the mutant and the wild-type, respectively, indicating that the molecules do not differ significantly from a sphere and the rotational diffusion is unlikely to be significantly anisotropic.

The dimensions and the orientation of the diffusion tensor of the two proteins were evaluated at every temperatures using the ^{15}N R_2/R_1 ratios and including only the residues used in the calculation of τ_m (*41*). The software R_2R_1_1.1 (*41*) was used to determine the diffusion tensors for spherical and axially symmetric motional modes. An axially symmetric model resulted to be more adequate than an isotropic model to describe the rotational diffusion of the wild-type thioredoxin at the three temperatures (F-statistics$_{(25°C)}$ = 3; F-statistics$_{(45°C)}$ = 3; F-statistics$_{(65°C)}$ = 16). At 25 °C, the protein adopts a prolate axially symmetric rotational diffusion model while an oblate axially symmetric rotational diffusion model (Dzz($\equiv D_{||}$) < Dxx = Dyy($\equiv D_{\perp}$)) gives better results at 45° and 65 °C (Table 3). The statistically best fit for the relaxation data (R_2/R_1 ratios) of the K18G/R82E BacTrx mutant, both at 25 and 45 °C, was obtained by using the axially symmetric model over the isotropic model (F-

Table 4: Model Selection Statistics[a]

BacTrx	25°C	45°C	65°C
model 1 (S^2_f)	31	59	65
model 2 (S^2_f,τ_e)	31	17	21
model 3 (S^2_f,R_{ex})	10	10	2
model 4 (S^2_f,τ_e,R_{ex})	7	5	1
model 5 (S^2_s, S^2_f,τ_e)	7	0	1
K18G/R82E BacTrx	**25 °C**	**45 °C**	**65 °C**
model 1 (S^2_f)	47	63	
model 2 (S^2_f,τ_e)	9	12	
model 3 (S^2_f,R_{ex})	25	14	
model 4 (S^2_f,τ_e,R_{ex})	5	3	
model 5 (S^2_s, S^2_f,τ_e)	1	1	

[a] Numbers of residues that fit to each of the five models are shown.

statistics$_{(25°C)}$ = 6; F-statistics$_{(45°C)}$ = 1.8); at 65 °C an isotropic diffusion model appears to be more appropriate (F-statistics$_{(65°C)}$ = 1). In particular, at 25 and 45 °C, the mutant protein adopts a prolate axially symmetric rotational diffusion model (Dzz($\equiv D_{||}$) > Dxx = Dyy($\equiv D_{\perp}$)) (Table 3). Furthermore, the program QUADRIC_DIFFUSION (*39*) was used to verify the possible improvement in the fully anisotropic model over axially symmetric diffusion, but the improvement was not statistically significant.

ModelFree Analysis. The measured relaxation data were used in the ModelFree software to determine the parameters characterizing the internal mobility. Five models (see Materials and Methods) were used to appropriately fit the dynamical parameters to the experimental relaxation data. The model selection strategy of Mandel and co-workers (*45*) was employed to select the correct model for each residue (Table 4). The calculated dynamics parameters (S^2, τ_e, and R_{ex}) versus the polypeptide sequence of the two proteins at the three different temperatures are reported in Figure 3a,b.

Alicyclobacillus acidocaldarius Thioredoxin. At 25 °C, the simple librational motion (model 1) suitably describes the dynamical behavior of merely a minor part (31 residues) of the protein H^N bond vectors; conversely, almost the half of residues show internal motion on the fast time scale (models 2 and 4). As it was expected, residues including a R_{ex} term are mainly located around the active site, the loops which are in closest contact with it and the α2 helix.

The global average S^2 value of 0.88 ± 0.08 is rather high, corresponding, in the representation of the "diffusion in a cone" (*47*, *57*, *58*), to a cone semi-angle of 16.6° and reflects the compact nature of the protein. The lowest S^2 values occur in the loop between α1 and β2 and in the last two turns of the C-terminal α-helix ($S^2_{(15-18)}$ = 0.78 ± 0.10 and $S^2_{(101-104)}$ = 0.78 ± 0.14). S^2 values lower than 0.7 are also observed for residue 51, which is located at the beginning of β3 strand and for residues 28 and 72, which are close to the active site.

At 45 °C, model 1 can be used to describe the dynamical behavior of a larger part of H^N bonds. Motions on the fast time scale (models 2 and 4) can be detected for 21 residues while an R_{ex} term is necessary for 15 H^N mainly located in the regions around the active site. At 65 °C, model 1 results to be appropriate for most of the residues even if 21 H^N present detectable motions on the fast time scale and an R_{ex} term is necessary for three residues. S^2 values slightly decrease with increasing temperature. The global average S^2 values at 45 and at 65 °C are 0.86 ± 0.05 and 0.82 ± 0.09, respectively.

As it is found at 25 °C, also at the higher temperatures the slowest S^2 values occur in the loop between α1 and β2 and at the C-terminus (at 65 °C, $S^2_{(15-18)}$ = 0.68 ± 0.23 and $S^2_{(101-104)}$ = 0.72 ± 0.09).

K18G/R82E BacTrx Mutant. At 25 °C, about half of the analyzed residues could be described by the simplest model of librational motion (model 1); a small number of residues are subject to internal motions on a rapid time-scale (model 2 and model 4), while a larger set requires a chemical exchange term (model 3 and 4). Only one residue (Asp102) presents motions on the slowest time-scale (model 5). The S^2 value averaged over the entire polypeptide chain is 0.88 ± 0.07, which corresponds to a cone semi-angle of 16.7°. As in the wild-type, the secondary structure elements present higher values of S^2 with respect to the loop regions (Figure 3a). The dynamic behavior of the α1β2 loop region, containing the Lys18Gly mutation, could be only partially described since residues 15 and 17 could not be fitted to the ModelFree formalism, probably because of too complicated motions. Nonetheless, S^2 of residues 16 and 18 are 0.59 and 0.68, respectively, which, being the lowest values along the amino acids sequence, indicate a pronounced flexibility of the backbone chain in this loop. On the contrary, the region around the mutation of residue 82 ($S^2_{(79-83)}$ = 0.89 ± 0.05) appears to be rather rigid. The dynamic behavior of the C-terminus is not comparable to that of the wild-type, since the residue 104 could not be fitted to any of the five models of the ModelFree analysis.

At 45 °C, the majority of residues could be fitted to model 1. Residues requiring an R_{ex} term are located in the regions around the active site (26−32), including the 25 and 28 tryptophan side-chains, at the end of the α3β4 loop around the residue 72 and in the β5α4 loop around residue 90. The average S^2 value of 0.83 ± 0.09 corresponding to a cone semi-angle of 20.0° shows a slight decrease in comparison to the value derived at 25 °C. The lowest S^2 values are found in the α1β2 loop ($S^2_{(15-18)}$ = 0.55 ± 0.23) and in the C-terminal tail ($S^2_{(101-104)}$ = 0.78 ± 0.06). Notably, residues 15 and 17 could be fitted to the ModelFree formalism, thus providing a complete picture of the internal mobility of this mutated loop at 45 °C.

At 65 °C, the majority of residues required an internal correlation time, so that the data could not be fitted to the ModelFree formalism at this temperature.

DISCUSSION

Structural Comparison. The K18G/R82E mutant of *A. acidocaldarius* thioredoxin shows the canonical thioredoxin motif (*19*, *55*) which also characterizes the wild-type structure (*14*). This fold is constituted by a central core of five β-strands forming a β-sheet and four helices and is characterized by two distinctive features. The first β-strand is actually rather disordered, as it is also observed in the NMR structure of thioredoxin m from Spinach (*16*); furthermore, the C-terminal α4 helix is divided into two helical segments, the first encompassing the residues 93−99 and the second including residues 101−104, even though these residues show a certain flexibility. The two helical portions have different orientation axes with the C-terminal α4 helix

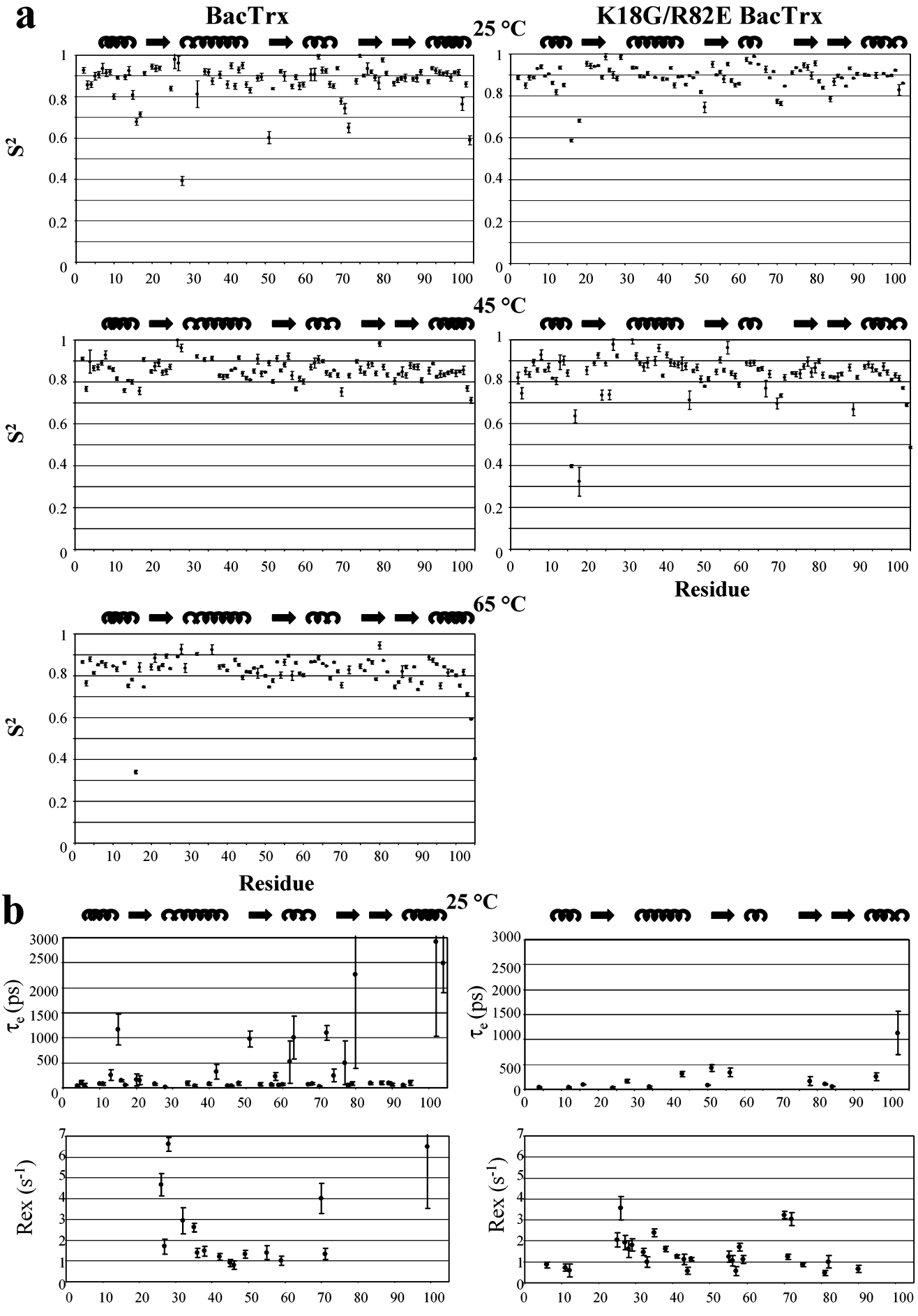
a
BacTrx
K18G/R82E BacTrx
25 °C
45 °C
65 °C
S²
Residue
b
25 °C
τe (ps)
Rex (s⁻¹)

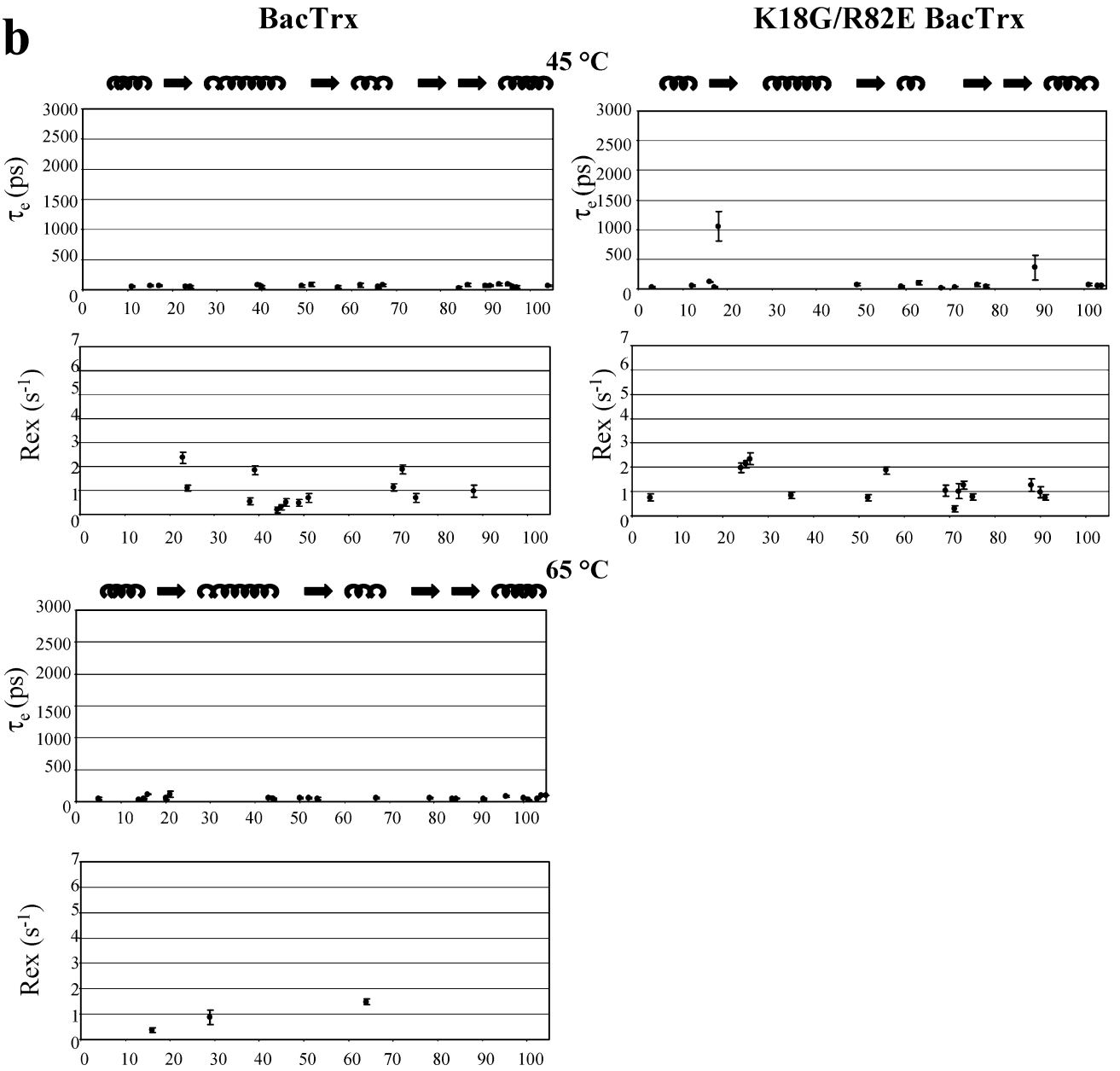

FIGURE 3: (a) Parameters defining the backbone dynamics of BacTrx and its K18G/R82E mutant. The order parameter, S^2, is plotted as a function of the residue numbers. (b) Parameters defining the backbone dynamics of BacTrx and its K18G/R82E mutant. The effective correlation time τ_e, and the chemical exchange term R_{ex} are plotted as functions of the residue numbers.

making a bend toward the α2−β3 loop region. This characteristic is also found in the structures of the single mutants which have been characterized by X-ray techniques (*54*).

The wild-type and mutant molecules show significant structural differences (backbone $rmsd_{(1-105)} = 1.38$ Å), which are localized not only in the more flexible loop regions, but also in the secondary structure elements (Figure 4a). In particular, the K18G/R82E BacTrx mutant structure shows a longer central β-sheet and a distorted C-terminal α4 helix (Figure 4b). The Thr51 amide proton is hydrogen bonded to Pro19 carbonyl oxygen, enlarging β2 and β3 strands of one residue; this structural feature is confirmed by the amide exchange rate of Thr51, which is sensibly slower in the double mutant than in the wild-type protein (see Supporting Information), as well as by the Thr51 S^2 value, which is remarkably higher in the double mutant (Figure 3a). At the same time, Arg82 amide proton is hydrogen bonded to the backbone carbonyl oxygen of Lys79, thus including those two residues in β5 and β4 strands, respectively. The one residue extension of β2, β3, β4, and β5 strands appears to be based on the loss of the electrostatic interactions involving the positively charged side-chain of Lys18; in the wild-type BacTrx, the Lys18(NZ)/Asp48(OD) ion pair connects the α1β2 loop to α2β3 one, which is, in turn, linked to the α4 helix through the Glu97(OE)/His46(HE1) salt bridge. This system of ion pairs, in the wild-type, causes the shortening of the central β-core, which seems a key feature, rendering the protein fold very compact and spherical; when Lys18 is substituted with a glycine, the system of ion pairs is broken and the central β-sheet recovers one residue. The extension of the core β-sheet is further stabilized by the mutation of Arg82, which causes the loss of the hydrogen bond between its positively charged side chain and Pro83 carbonyl oxygen,

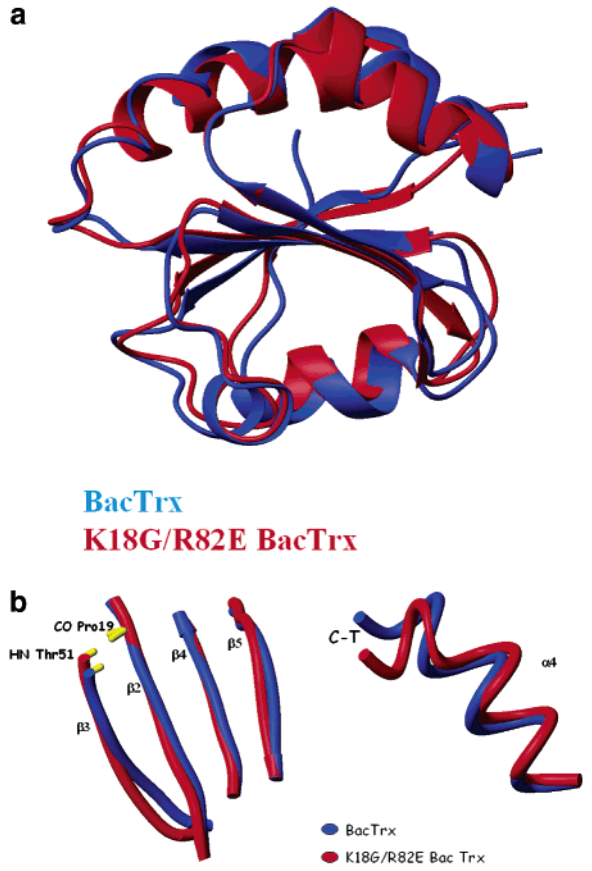

FIGURE 4: (a) Superposition for minimal rmsd of the backbone atoms of the BacTrx (blue) with its K18G/R82E mutant (red). (b) Comparison of the secondary structure elements of BacTrx (blue) and its K18G/R82E mutant (red): superimposition for minimal rmsd of the β-strands 2, 3, 4, and 5 (left), and of the helices 4 (right).

observed in the wild-type structure, allowing the Arg82 to assume an extended conformation and its backbone amide proton to form a hydrogen bond with Lys79 carbonyl oxygen.

Figure 4b also shows that the C-terminal portion of α4 helix is distorted in the double mutant protein structure. This helix plays an important structural role in the *A. acidocaldarius* thioredoxin being linked, mainly by electrostatic interaction, to the adjacent α2 helix. Intrahelical ion-pairs are important stabilizing factors of helices in proteins from thermophile (*59*). Furthermore, α4 helix plays a protecting role toward the central core to which it is joined through hydrophobic and electrostatic contact mainly localized within the β5 strand (*14*). The helix distortion seems to be due to the weakening of the packing between the helix and the β-sheet, presumably caused by the stretching of the central core. In particular, the electrostatic interaction between Lys85 (β5) and Asp102 (α4) side chains is strongly reduced in favor of the formation of a hydrogen bond between Lys85 side chain and Gln99 backbone carbonyl, which causes the breaking of the α4 helix secondary structure. On the other hand, the bend of the C-terminal portion toward the α2β3 loop results in stabilizing interactions between the positively charged Lys49 side chain and Leu104 and/or Gln105 backbone carbonyls.

In Table 5, relevant structural features, which are related to the thermal stability of a protein (*60*), are compared, as they are found in the thioredoxin from the mesophile *E. coli* (X-ray structure, PDB code 2TRX), in the thioredoxin from

Table 5: Comparison of Structural Features in *Escherichia coli*, *Alicyclobacillus acidocaldarius*, and K18G/R82E *Alicyclobacillus acidocaldarius* Thioredoxins

	EcTrx (2TRX)	BacTrx (1QUW)	K18G/R82E BacTrx
no. of residues in α-helix	32 (0.30)	41 (0.39)	33 (0.31)
no. of residues in β-sheet[a]	25 (0.23)	22 (0.21)	25 (0.24)
ion pairs (4 Å)	7 (0.06)	4 (0.04)	5 (0.05)
ion pairs (7 Å)	17 (0.16)	17 (0.16)	12 (0.11)

[a] Those of the more disordered β1 strand are not included.

the moderate thermophile *A. acidocaldarius* (NMR structure, PDB code 1QUW) and in the K18G/R82E mutant. As it is clearly evident, the two mutations strongly affect the structural properties of the thermostable thioredoxin, making the secondary structure elements of the double mutants, more similar to those of the mesophilic *E. coli* protein. In particular, the comparison of the secondary structure elements reveals an increase of residues in the β-sheet and a decrease of the residues in α-helices of the mutant protein, in a very good agreement with the circular dichroism analysis of the two proteins (*22*). In particular, the β3 and β5 strands are one residue longer at the N-terminus, while the β4 is one residue longer at the C-terminus; on the contrary, the helix α1 is two residues longer in the wild-type thioredoxin including residues 7 and 15 and the α3 helix, which in the wild-type thioredoxin extends from the residue 62 to the residue 67, in the double mutant does not properly form (Figure 1a). The shortening of the α-helices clearly reduces their capability to protect the protein core from the solvent environment, facilitating the unfolding processes. As it has been described (*14*), a relevant number of ion-pairs contribute to the stabilization of the global fold of BacTrx. In the K18G/R82E BacTrx mutant the number of long-range ion-pairs (Table 5) is strongly reduced, so affecting the overall electrostatic energy of the molecule. Indeed, the short-range salt-bridges Glu41(OE)/Lys93(NZ), Asp102(OD)/Lys85(NZ) and the long-range Glu97(OE)/His46(NE), which are important in joining the C-terminal helix α4 to α2 and β5, are conserved in the mutant.

Backbone Dynamics. In the present study, we have also analyzed the backbone dynamics of both the *A. acidocaldarius* thioredoxin and its K18G/R82E mutant in a wide temperature range from 25 °C up to 65 °C, so including the growth temperature of the bacterium, which is between 55 and 65 °C (*61*). Even if many studies have been published that report protein backbone dynamics studies as function of temperature (*62*−*71*), a minor part of them were focused on the mobility of thermostable proteins analyzed in a range comprising the temperature range of growth of their sources.

In particular, Bertini and co-workers have described a ModelFree analysis of a thermophilic Fe_7S_8 protein compared with a mesophilic Fe_4S_4 protein (*66*). This study reveals that no relevant differences are observable in the order parameters of the two proteins at room temperature and that, noticeably, the backbone dynamics of the thermophilic protein retain a relevant rigidity when the temperature is increased to 54 °C.

Here we have explored the temperature-dependent dynamic behavior of two thermostable proteins, one of them with reduced thermostability after a design in silico (*22*), in

a range that includes the temperature at which the wild-type protein performs its function in vivo.

The trend of the relaxation parameters and of the heteronuclear ^{15}N-{^{1}H}-NOE values of the two proteins at the three different temperatures essentially depends on the secondary structure architecture of the protein scaffold. The analysis of the average R_1 and R_2 values of the two proteins, along the examined temperature range, reveals that they are rather similar (Table 2); on the contrary, significant differences are detected in the average NOE values, which, at 65 °C, are sensibly lower in the mutant protein, thus indicating a clear increase of large amplitude internal motions.

Aiming to gain a more quantitative description, we have evaluated the microdynamic parameters characterizing internal motions by performing a ModelFree analysis. As a first step, we estimated the axially symmetric diffusion tensor of the molecules as the best fitting the collected relaxation data. This diffusional mode has been recently chosen in a backbone dynamics study of a chimeric human−*E. coli* thioredoxin (*17*) while earlier studies carried out on *E. coli* thioredoxin (*18*) and on the thioredoxin from green alga (*15*) adopted an isotropic diffusion tensor.

All the five different models of motion have been tested as described in Materials and Methods for each of the residues. At 25 °C, only a minor part of residues of the wild-type could be fitted with the simplest model 1 and an equal number of residues required an internal correlation time, faster than the global correlation time. The remaining residues, slightly less than one-third, are well distributed among the other three models. On the contrary, at 25 °C the majority of residues of the double mutant could be fitted with model 1 even though a significant number required an R_{ex} term (Table 4). These results indicate a different time scale of the HN vector motions of the two proteins at room temperature: while the wild-type protein presents detectable internal motions mainly in the pico- to nanosecond and, to a lesser extent, in the milli- to microsecond time scale (those latter are concentrated in the active site), motions in the milli- to microsecond time scale seems to determine the dynamical behavior of the double mutant. When the temperature is raised to 45 °C, the internal motions of both the proteins become more homogeneous and mainly described with model 1 and noticeably reduced differences of internal dynamics are observed between the two proteins.

At 65 °C, the wild-type protein shows a more uniform dynamical behavior of the HN vectors, presenting more than two-thirds of the residues that can be analyzed with model 1, whereas almost all the remaining residues require an effective correlation time. Interestingly, the analysis of the relaxation data of the K18G/R82E BacTrx mutant at the same temperature, once performed the model selection strategy (*48*), cannot be completed, because of high errors in microdynamic parameters and no statistically significant results. Indeed, at 65 °C the average NOE value already indicates a large amplitude of the internal motions; not surprisingly, during the ModelFree analysis, the large majority of double mutant HN vectors requires an internal correlation time, thus causing the failure of the ModelFree approach (*42*, *46*). This behavior is not so unexpected since a considerable number of previous studies carried out at different temperatures already failed to use the ModelFree approach at the highest values of the temperature range (*64*, *72*−*74*). On the other side, it is remarkable that the ModelFree analysis of the wild-type protein relaxation data acquired at 65 °C, which is in the growth temperature range of *A. acidocaldarius*, shows that the wild-type protein retains considerable rigidity. In particular, the average value of the square of the generalized order parameter decreases slightly with temperature, going from 0.88 at 25 °C to 0.82 at 65 °C (Table 2), indicating only a modest increase in the amplitude of internal motions (about 4°, using the model of diffusion in a cone). On the contrary, a different behavior characterizes the backbone dynamics of the double mutant, whose average value of S^2 diminishes from 0.88 at 25 °C to 0.83 at 45 °C and is not assessable at 65 °C, very likely because of a too large increase of the internal motion amplitudes.

The inspection of the trend of the S^2 value along the peptide chain of the two protein at the different temperatures (Figure 3a) reveals that, as expected, the highest HN vector rigidity is found in the secondary structure elements, with the only exception of the last segment of the C-terminal helix, which is less rigid. On the other side, the loop regions are generally more flexible, in particular, the $\alpha1\beta2$ loop and less markedly the $\alpha3\beta4$ loop, which is not far from the active site. These two loop regions are similarly flexible in the two proteins at 25 °C. Interestingly, the $\alpha1\beta2$ loop becomes sensibly more flexible in the double mutant at 45 °C, as well as the last portion of the final $\alpha4$ helix. The dynamic behavior of these two regions of the double mutant appears to be very sensible to the temperature increase, whereas in the wild-type protein they substantially retain their rigidity up to 65 °C. The S^2 diagram of the wild-type protein at 65 °C shows that at that temperature the protein backbone is still rather rigid; in particular, the average S^2 value is still high and none of the loop regions show a sensibly increased flexibility, so testifying the high thermal resistance of the *A. acidocaldarius* wild-type thioredoxin.

In Figure 3b, the effective internal correlation times (τ_e) and exchange terms (R_{ex}) required for residues of both the proteins at the three temperatures are also reported. Remarkably, the highest internal correlation times are requested for the wild-type at 25 °C; furthermore, the residues that show motions in the pico- to nanosecond range are quite well distributed over the entire backbone chain. Recent studies suggest that the local internal motions may increase the stability by increasing the entropy of native state (*75*). More recent molecular dynamics studies of laboratory evolved thermophilic enzymes indicate that an increase of protein internal motions in the nano- to picosecond time scale characterizes the two thermostable variants in comparison to the wild-type protein (*76*). These findings are significantly confirmed by our study, which indicates that the wild-type protein at 25 °C presents a large number of local internal motions in the range of nano- to picosecond time scale. These local motions decrease with the increase of the temperatures, becoming at 65 °C, which is very close to the optimal growth temperature of the thermophilic bacterium (*61*), more comparable to what is observed in the mesophilic *E. coli* thioredoxin at room temperature. Not surprisingly, the less stable double mutant shows less internal fast motions, which at 45 °C are comparable to those observed in the wild-type at 65 °C. Less marked differences are observed in the residues requiring the exchange terms for the two proteins; they are mostly located close to the active site of the two

proteins and strongly decrease with the temperature increase.

Comparison with Previous Backbone Mobility Studies of Thioredoxins. Backbone dynamics studies carried out by means of ^{15}N relaxation measurements and ModelFree analysis have already been reported for thioredoxins from mesophilic sources such as *E. coli* (*18*) and the green alga (*15*); moreover, backbone dynamics studies of the chimeric human−*E. coli* thioredoxin (*17*), which exhibits reduced thermostability with respect to the two parent proteins (*77*), have been recently described.

^{15}N relaxation measurements of *E. coli* thioredoxin have been performed at 35 °C. The authors adopt an isotropic diffusion model of the molecule and obtain an average S^2 value of 0.86 (0.01). The regions with the lowest S^2 values were found to be mainly localized close to the N- and C-terminus, in the two loops which are in contact with the active site, and the loop around α1 and β2, i.e., the region where the mutation of residue 18 occurs in the K18G/R82E mutant of *A. acidocaldarius*, which are the same regions where the higher flexibility either for the wild-type and for the mutant is also observed. Furthermore, residues requiring the R_{ex} term are mainly located in the region around the active site, and our results are again in agreement with these findings. Backbone dynamics studies of thioredoxin from the green alga have been carried out at 38 °C. The authors, assuming an isotropic rotational diffusion tensor of the molecule, attain an average S^2 value of 0.84 (0.09), and the majority of residues could be fitted with the simplest model of librational motion (model 1) without great differences respect to *E. coli* thioredoxin as concerning the residues including a τ_e or an R_{ex} term. Finally, the chimeric human−*E. coli* thioredoxin backbone dynamics have been studied at 35 °C. In this study, the authors find that an axially symmetric diffusor tensor describes relaxation data better than an isotropic one, as we have found out for *A. acidocaldarius* thioredoxin. The global average S^2 resulted as 0.88, and most of the residues could be fitted to model 1. Residues exhibiting lower S^2 values are located in loops or at the C-terminus and show a motional behavior similar to that observed for *E. coli* thioredoxin.

A detailed comparison of those previous studies with our backbone dynamics studies on *A. acidocaldarius* is hampered by the different experimental conditions used. Nonetheless, some important key points can be evaluated: (i) The average order parameter of the all thioredoxins analyzed so far at room temperature is substantially constant, demonstrating an intrinsic very compact nature of the thioredoxin fold. (ii) The most flexible region is regularly found in the α1β2 loop while the active site appears to be characterized by motions in the micro- to millisecond time scale of the backbone chain. Our findings introduce supplementary data regarding the nature of the backbone mobility of two thermostable thioredoxins at higher temperature. Of a considerable interest is the capacity of the wild-type protein to largely retain its rigidity features also at the highest temperature, which lies in the growth temperature range of its source. Intriguingly, the less thermostable double mutant tends to lose its structural rigidity at upper temperatures, exhibiting a very high mobility of the α1β2 loop, where the first mutation occurred, already at 45 °C.

Molecular and Dynamic Bases of the Different Thermostability. Previous studies carried out on the homology model of *A. acidocaldarius* thioredoxin and on its NMR structure (*20*, *14*) have suggested that the increased thermostability of BacTrx with respect to its mesophilic homologue (*E. coli* thioredoxin) is achieved by several improvements at many locations within the protein structure. Although many features have been proposed as structural determinants of *A. acidocaldarius* thioredoxin thermostability (e.g., the presence of two additional Pro residues in loops which reduces the entropy of the unfolded state; favorable charged residues stabilizing the macrodipole of α1 and α2; a shorter N-terminus thus decreasing the flexibility of this region which in turn is joined to the rigidity of the C-terminus due to the multiple interactions involving α4), a thermodynamic stability study of *A. acidocaldarius* thioredoxin mutants, designed on the basis of molecular dynamic simulations, has revealed that major contributions to thermostability derive from electrostatic interactions occurring on the protein surface (*21*, *22*). In particular, by substituting the residues involved in such electrostatic interactions, Lys18 and Arg82, with a Gly and a Glu (which are the residues located at the corresponding positions in the *E. coli* thioredoxin), respectively, significantly less thermostable mutants were obtained (*21*). Furthermore, the reversal substitution of the second mutation in *E. coli* thioredoxin causes a remarkable increase of the thermal resistance, confirming the relevance of those interactions in modulate the thioredoxin thermostability (*23*). Recently, an integrated structural and computational study on the thermostability of the two single point mutants, Lys18Gly and Arg82Glu of the *A. acidocaldarius* thioredoxin, pointed out that those two single mutations affect the whole electrostatic energy of the two molecules, causing the reduction of the thermostability (*54*).

Our study has regarded the solution structure and the temperature-dependent dynamic behavior of the double mutant Lys18Gly/Arg82Glu of the *A. acidocaldarius* thioredoxin. Our findings clearly show that the insertion of the two mutations cause a loss of energetically favorable long-range interactions (Table 5), which alter the very compact and spherical folding of the thermophilic thioredoxin. In particular, we observe the stretching of the β-sheet core and a consistent reduction of the length of the α-helices, which renders the secondary structure elements of the double mutants more similar to those of the mesophilic *E. coli* thioredoxin. Therefore, the electrostatic interactions, in which Lys18 and Arg82 are involved on the surface of the thermostable thioredoxin, appear to be fundamental in maintaining the protein structure stable at high temperature.

Here we have also presented the first comparison of the temperature-dependent backbone dynamics of a thermophilic protein, the *A. acidocaldarius* thioredoxin, with that of a less thermostable in silico designed mutant. The protein dynamics analysis has covered a wide temperature range, which includes the growth temperature range of *A. acidocaldarius.* The order parameter trends of the two proteins are rather similar to those of the previously analyzed mesophilic thioredoxins at room temperature; when the temperature is increased the wild-type retains almost completely its global dynamics, while parts of the double mutant become more flexible. In particular, at 65 °C, which is in the optimal growth temperature of its source, the BacTrx is globally as rigid as the mesophilic thioredoxins are at room temperature; on the contrary, at 65 °C, the K18G/R82E BacTrx mutant

is characterized by a large decrease of the average heteronuclear ^{15}N-{^{1}H}-NOE value and the relaxation data could not be fitted by the ModelFree analysis, very likely because of too large increase of the amplitude of the internal motions. Furthermore, a considerable number of BacTrx backbone HN vectors shows internal motions in the pico- to nanosecond time scale particularly at room temperature. Clearly, certain modes of motions, in particular those that may initiate unfolding, need to be reduced if a protein has to achieve stability at high temperatures; nonetheless, other types of motions, such as those observed in BacTrx, may be not detrimental to the protein stability, but, on the contrary, they may provide an entropic advantage to the native state (*76*). Intriguingly, those kind of motions tend to be reduced at the highest temperatures in the wild-type and are generally less present in the double mutant.

This study further confirms that protein thermostability is reached through diverse stabilizing interactions, which have the key role to maintain the structural folding stable and functional at the working temperature. Moreover, our research verifies that structural and dynamic analyses of thermostable proteins modified to decrease their heat resistance, as well as of laboratory-evolved thermostable variants of mesophilic proteins, represent an important way to better identify the molecular and dynamic bases of protein thermal stability.

ACKNOWLEDGMENT

NMR spectra were recorded at the European Research Infrastructure 'Center for Design and Structure in Biology' (CDSB) at the Institut für Molekulare Biotechnologie (IMB) in Jena, Germany. The authors thank Claudia Florio and Francesco Pellegrino which gave valuable contributions to the scientific work. The authors also thank Dr. R. Ramachandran (IMB) for helpful discussions and experimental support and Mr. Leopoldo Zona, Mr. Maurizio Muselli and Mr. Marco Mammucari for the excellent technical assistance.

SUPPORTING INFORMATION AVAILABLE

Tables reporting the values and uncertainties of the experimentally determined R_1, R_2, NOE, and ModelFree dynamics parameters (order parameters S^2, effective correlation times τ_e, and exchange broadening term R_{ex}) for both BacTrx and the K18G/R82E BacTrx mutant at 25, 45, and 65 °C. Figure 5 showing slow exchanging amide protons as detected in 2D [^{1}H,^{15}N] HSQC spectrum of BacTrx and its K18G/R8E mutant, recorded 24 h after the dissolution of the proteins in pure $^{2}H_2O$.

REFERENCES

1. Jaenicke R. (1991) Protein stability and molecular adaptation to extreme conditions. *Eur. J. Biochem. 202*, 715−728.
2. Jaenicke, R., and Böhm, G. (1998) The stability of proteins in extreme environments. *Curr. Opin. Struct. Biol. 8*, 738−748.
3. Creighton, T. E. (1993) *Proteins: Structure and Molecular Properties*, W. H. Freeman, New York.
4. Fersht, A. (1999) *Structure and Mechanism in Protein Science*, W. H. Freeman, New York.
5. Yano, J. K., and Poulos, T. L. (2003) New understandings of thermostable and peizostable enzymes. *Curr. Opin. Biotechnol. 14*, 360−365.
6. Zavodsky, P., Kardos, J., Svingor, A., and Petsko, G. A. (1998) Adjustment of conformational flexibility is a key event in the thermal adaptation of proteins. *Proc. Natl. Acad. Sci. U.S.A. 95*, 7406−7411.
7. Perl, D., and Schmid, F. X. (2001) Electrostatic stabilization of a thermophilic cold shock protein. *J. Mol. Biol. 313*, 343−357.
8. Holmgren, A. (1985) Thioredoxin. *Annu. Rev. Biochem. 54*, 237−271.
9. Katti, S. K., LeMaster, D. M., and Eklund, H. (1990) Crystal structure of thioredoxin from *Escherichia coli* at 1.68 Å resolution. *J. Mol. Biol. 212*, 167−184.
10. Holmgren, A., Söderberg, B. O., Eklund, H., and Branden, C. I. (1975) Three-dimensional structure of *Escherichia coli* thioredoxin-S2 to 2.8 Å resolution. *Proc. Natl. Acad. Sci. U.S.A. 72*, 2305−2309.
11. Qin, J., Clore, G. M., and Gronenborn, A. M. (1994) The high-resolution three-dimensional solution structures of the oxidized and reduced states of human thioredoxin. *Structure 2*, 503−522.
12. Jeng, M. F., Campbell, A. P., Begley, T., Holmgren, A., Case, D. A., Wright, P. E., and Dyson, H. J. (1994) High-resolution solution structures of oxidized and reduced *Escherichia coli* thioredoxin. *Structure 2*, 853−868.
13. Mittard, V., Blackledge, M. J., Stein, M., Jacquot, J. P., Marion, D., and Lancelin, J. M. (1997) NMR solution structure of an oxidised thioredoxin h from the eukaryotic green alga *Chlamydomonas reinhardtii*. *Eur. J. Biochem. 243*, 374−383.
14. Nicastro, G., De Chiara, C., Pedone, E., Tato, M., Rossi, M., and Bartolucci, S. (2000) NMR solution structure of a novel thioredoxin from *Bacillus acidocaldarius* possible determinants of protein stability. *Eur. J. Biochem. 267*, 403−413.
15. Lancelin, J. M., Guilhaudis, L., Krimm, I., Blackledge, M. J., Marion, D., and Jacquot, J. P. (2000) NMR structures of thioredoxin m from the green alga *Chlamydomonas reinhardtii*. *Proteins 41*, 334−349.
16. Neira, J. M., Gonzales, C., Toiron, C., De Prat-Gay, G., and Rico, M. (2001) Three-dimensional solution structure and stability of thioredoxin m from spinach. *Biochemistry 40*, 146−156.
17. Dangi, B., Dobrodumov, A. V., Louis, J. M., and Gronenborn, A. M. (2002) Solution structure and dynamics of the human-*Escherichia coli* thioredoxin chimera: insights into thermodynamic stability. *Biochemistry 41*, 9376−9388.
18. Stone, M. J., Chandrasekhar, K., Holmgren, A., Wright, P. E., and Dyson, H. J. (1993) Comparison of backbone and tryptophan side-chain dynamics of reduced and oxidized *Escherichia coli* thioredoxin using ^{15}N NMR relaxation measurements. *Biochemistry 32*, 426−435.
19. Eklund, H., Gleason, F. K., and Holmgren, A. (1991) Structural and functional relations among thioredoxins of different species. *Proteins 11*, 13−28.
20. Bartolucci, S., Guagliardi, A., Pedone, E., De Pasquale, D., Cannio, R., Camardella, L., Rossi, M., Nicastro, G., De Chiara, C., Facci, P., Mascetti, G., and Nicolini, C. (1997) Thioredoxin from *Bacillus acidocaldarius*: characterization, high-level expression in *Escherichia coli* and molecular modelling. *Biochem. J. 328*, 277−285.
21. Pedone, E., Bartolucci, S., Rossi, M., and Saviano, M. (1998) Computational analysis of the thermal stability in thioredoxins: a molecular dynamics approach. *J. Biomol. Struct. Dyn. 16*, 437−446.
22. Pedone, E., Cannio, R., Saviano, M., Rossi, M., and Bartolucci, S. (1999) Prediction and experimental testing of *Bacillus acidocaldarius* thioredoxin stability. *Biochem. J. 339*, 309−317.
23. Pedone, E., Saviano, M., Rossi, M., and Bartolucci, S. (2001) A single point mutation (Glu85Arg) increases the stability of the thioredoxin from *Escherichia coli*. *Protein Eng. 14*, 255−260.
24. Zhang, O., Kay, L. E., Olivier, J. P., and Forman-Kay, J. D. (1994) Backbone ^{1}H and ^{15}N resonance assignments of the N-terminal SH3 domain of drk in folded and unfolded states using enhanced-sensitivity pulsed field gradient NMR techniques. *J. Biomol. NMR 4*, 845−858.
25. Talluri, S., and Wagner, G. (1996) An optimized 3D NOESY-HSQC. *J. Magn. Reson. 112*, 200−205.
26. Vuister, G. W., and Bax, A. (1993) A. Quantitative J correlation: a new approach for measuring homonuclear three-bond J(HNHα) coupling constants in ^{15}N-enriched proteins. *J. Am. Chem. Soc. 115*, 7772−7777.
27. Archer, S. J., Ikura, M., Torchia, D. A., and Bax, A. (1991) An alternative 3D-NMR technique for correlating backbone N-15 with

side chain H-beta-resonances in larger proteins. *J. Magn. Reson. 95*, 636−641.
28. Wilker, W., Leibfritz, D., Kerssebaum, R., and Bermel, W. (1993) Gradient selection in inverse heteronuclear correlation spectroscopy. *Magn. Reson. Chem. 31*, 287−292.
29. Griesinger, C., Otting, G., Wüthrich, K., and Ernst, R. R. (1988) Clean TOCSY for ^{1}H spin system identification in macromolecules. *J. Am. Chem. Soc. 110*, 7870.
30. Kumar, A., Ernst, R. R., and Wüthrich, K. (1980) A two-dimensional nuclear Overhauser enhancement (2D NOE) experiment for the elucidation of complete proton−proton cross-relaxation networks in biological macromolecules. *Biochem. Biophys. Res. Commun. 95*, 1−6.
31. Rance, M., Sörensen, O. W., Bodenhausen, G., Wagner, G., Ernst, R. R., and Wüthrich, K. (1983) Improved spectral resolution in COSY ^{1}H NMR spectra of proteins via double quantum filtering. *Biochem. Biophys. Res. Commun. 117*, 479−485.
32. Cavanagh, J., and Rance, M. (1992) Suppression of Cross-Relaxation Effects in TOCSY Spectra Via a Modified Dipsi-2 Mixing Sequence. *J. Magn. Reson. 96*, 670−678.
33. Kay, L. E., Keifer, P., and Saarinen, T. (1992) Pure absorption gradient enhanced heteronuclear single quantum correlation spectroscopy with improved sensitivity. *J. Am. Chem. Soc.114*, 10663−10665.
34. Bartels, C., Xia, T., Billeter, M., and Wüthrich, K. (1995) The program XEASY for computer-supported NMR spectral analysis of biological macromolecules. *J. Biomol. NMR 5*, 1−10.
35. Farrow, N. A., Muhandiram, R., Singer, A. U., Pascal, S. M., Kay, C. M., Gish, G., Shoelson, S. E., Pawson, T., Forman-Kay, J. D., and Kay, L. E. (1994) Backbone dynamics of a free and phosphorpeptidecomplexed Src homology 2 domain studied by ^{15}N NMR relaxation. *Biochemistry 33*, 5984−6003.
36. Shapiro, Y. E., Sinev, M. A., Sineva, E. V., Tugarinov, V., and Meirovitch E. (2000) Backbone dynamics of *Escherichia coli* Adenylate Kinase at the Extreme Stages of the Catalytic Cycle Studied by ^{15}N NMR Relaxation. *Biochemistry 39*, 6634−6644.
37. Beeser, S. A., Goldenberg, D. P., and Oas, T. G. (1997) Enhanced Protein Flexibility Caused by a Destabilizing Amino Acid Replacement in BPTI. *J. Mol. Biol. 269*, 154−164.
38. Viles, J. H., Duggan, B. M., Zaborowski, E., Schwarzinger, S., Huntley, J. J. A., Kroon, G. J. A., and Dyson, H. J. (2001) Potential bias in NMR relaxation data introduced by peak intensity analysis and curve fitting methods. *J. Biomol. NMR 21*, 1−9.
39. Lee, L. K., Rance, M., Chazin, W. J., and Palmer, A. G. (1997) Rotational diffusion anisotropy of proteins from simultaneous analysis of ^{15}N and ^{13}Cα nuclear spin relaxation. *J. Biomol. NMR 9*, 287−298.
40. Brüschweiler, R., Liao, X., and Wright, P. E. (1995) Long-range motional restrictions in a multidomain zinc-finger protein from anisotropic tumbling. *Science 268*, 886−889.
41. Tjandra, N., Feller, S. E., Pastor, R. W., and Bax, A. (1995) Rotational diffusion anisotropy of human ubiquitin from ^{15}N NMR relaxation. *J. Am. Chem Soc. 117*, 12562−12566.
42. Lipari, G., and Szabo, A. (1982) Model-free approach to the interpretation of nuclear magnetic resonance relaxation in macromolecules. Theory and range of validity. *J. Am. Chem. Soc. 104*, 4546−4559.
43. Clore, G. M., Driscoll, P. C., Wingfield, P. T., and Gronenborn, A. M. (1990) Analysis of the backbone dynamics of interleukin-1 beta using two-dimensional inverse detected heteronuclear ^{15}N-^{1}N NMR spectroscopy. *Biochemistry 29*, 7387−7401.
44. Barbato, G., Ikura, M., Kay, L. E., Pastor, R. W., and Bax, A. (1992) Backbone dynamics of calmodulin studied by ^{15}N relaxation using inverse detected two-dimensional NMR spectroscopy: The central helix is flexible. *Biochemistry 31*, 5269−5278.
45. Mandel, A. M., Akke, M., and Palmer, A. G. (1995) Backbone dynamics of *Escherichia coli* ribonuclease HI: correlations with structure and function in an active enzyme. *J. Mol. Biol. 246*, 144−163.
46. Lipari, G., and Szabo A. (1982) Model-free approach to the interpretation of nuclear magnetic resonance relaxation in macromolecules. Analysis of experimental results. *J. Am. Chem. Soc. 104*, 4559−4570.
47. Clore, G. M., Szabo, A., Bax, A., Kay, L. E., Driscoll, P. C., and Gronenborn, A. M. (1990) Deviations from the simple two-parameter model-free approach to the interpretation of nitrogen-15 nuclear magnetic relaxation of proteins. *J. Am. Chem. Soc. 112*, 4989−4991.
48. Palmer, A. G., Rance, M., and Wright, P. E. (1991) Intramolecular motions of a zinc finger DNA-binding domain from xfin characterized by proton-detected natural abundance ^{13}C heteronuclear NMR spectroscopy. *J. Am. Chem. Soc. 113*, 4371−4380.
49. Herrmann, T., Güntert, P., and Wüthrich, K. (2002) Protein NMR structure determination with automated NOE assignment using the new software CANDID and the torsion angle dynamics algorithm DYANA. *J. Mol. Biol. 319*, 209−227.
50. Luginbühl, P., Güntert, P., Billeter, M., and Wüthrich, K. (1996) The new program OPAL for molecular dynamics simulations and energy refinements of biological macromolecules. *J. Biomol. NMR 8*, 136−146.
51. Koradi, R., Billeter, M., and Wüthrich, K. (1996) MOLMOL: a program for display and analysis of macromolecular structures. *J. Mol. Graphics 14*, 29−32.
52. Laskowski, R. A., Rullmann, J. A., MacArthur, M. W., Kaptein, R., and Thornton, J. M. (1996) AQUA and PROCHECK-NMR: programs for checking the quality of protein structures solved by NMR. *J. Biomol. NMR 8*, 477−486.
53. Güntert, P., Mumenthaler, C., and Wüthrich, K. (1997) Torsion angle dynamics for NMR structure calculation with the new program DYANA. *J. Mol. Biol. 273*, 283−298.
54. Bartolucci, S., De Simone, G., Galdiero, S., Improta, R., Menchise, V., Pedone, C., Pedone, E., and Saviano, M. (2003) An integrated structural and computational study of the thermostability of two thioredoxin mutants from *Alicyclobacillus acidocaldarius*. *J. Bacteriol. 185*, 4285−4289.
55. Martin, J. L. (1995) Thioredoxin a fold for all reasons. *Structure 15*, 245−250.
56. Kay, L. E., Torchia, D. A., and Bax, A. (1989) Backbone dynamics of proteins as studied by nitrogen-15 inverse detected heteronuclear NMR spectroscopy: application to staphylococcal nuclease. *Biochemistry 28*, 8972−8979.
57. Lipari, G., and Szabo, A. (1980) Effect of librational motions on fluorescemce depolarization and nuclear magnetic resonance relaxation in macromolecules and membranes. *Biophys. J. 30*, 489−506.
58. Lipari, G., and Szabo, A. (1981) Pade approximant to correlation function for restricted rotational diffusion. *J. Chem. Phys. 75*, 2971−2976.
59. Chakravarty, S., and Varadarajan, R. (2002) Elucidation of factors responsible for enhanced thermal stability of proteins: a structural genomics based study. *Biochemistry 41*, 8152−8161.
60. Szilagyi, A., and Zavodszky, P. (2000) Structural differences between mesophilic, moderately thermophilic and extremely thermophilic protein subunits: results of a comprehensive survey. *Struct. Folding Des. 8*, 493−504.
61. Darland, G., and Brock, T. D. (1971) *Bacillus acidocaldarius* sp. nov, an acidophilic thermophilic spore-forming bacterium. *J. Gen. Microbiol. 67*, 9−15.
62. Mandel, A. M., Akke, M., and Palmer, A. G. (1996) Dynamics of ribonuclease H temperature dependence of motions on multiple time scales. *Biochemistry 35*, 16009−16023.
63. Landry, S. J., Steede, N. K., and Maskos, K. (1997) Temperature dependence of backbone dynamics in loops of human mitochondrial heat shock protein 10. *Biochemistry 36*, 10975−10986.
64. Bracken, C., Carr, P. A., Cavanagh, J., and Palmer, A. G. (1999) Temperature dependence of intramolecular dynamics of the basic region leucine zipper of GCN4: implications for the entropy of association with DNA. *J. Mol. Biol. 285*, 2133−2146.
65. Evenäs, J., Forsén, S., Malmendal, A., and Akke, M. (1999) Backbone dynamics and energetics of a calmodulin domain mutant exchanging between closed and open conformations. *J. Mol. Biol. 289*, 603−617.
66. Bertini, I., Luchinat, C., Niikura, Y., and Presenti, C. (2000) Model-Free Analysis of a Thermophilic Fe_7S_8 Protein Compared with a Mesophilic Fe_4S_4 Protein. *Proteins 41*, 75−85.
67. Seewald, M. J., Pichumani, K., Stowell, C., Tibbals, B. V., Regan, L., and Stone, M. J. (2000) The role of backbone conformational heat capacity in protein stability: temperature-dependent dynamics of the B1 domain of Streptococcal protein G. *Protein Sci. 9*, 1177−1193.
68. Lee, A. L., Sharp, K. A., Kranza, J. K., Song, X., and Wand, A. J. (2002) Temperature dependence of the internal dynamics of a calmodulin-peptide complex. *Biochemistry 41*, 13814−13825.
69. Vugmeyster, L., Trott., O., McKnight, C. J., Raleigh, D. P., and Palmer, A. G., III (2002) Temperature-dependent dynamics of the villin headpiece helical subdomain, an unusually small thermostable protein. *J. Mol. Biol. 320*, 841−854.

70. Idiyatullin, D., Nesmelova, I., Daragan, V. A., and Mayo, K. (2003) Heat capacities and a snapshot of the energy landscape in protein GB1 from the Pre-denaturation temperature dependence of backbone NH nanosecond fluctuations. *J. Mol. Biol. 325*, 149−162.
71. Kovrigin, E. L., Cole, R., and Loria, J. P. (2003) Temperature dependence of the backbone dynamics of Ribonuclease A in the ground state and bound to the inhibitor 5′-phosphorhymidine (3′-5′)pyrophosphatase adenosine 3′-phosphate. *Biochemistry 42*, 5279−5291.
72. Bhattacharya, S., Falzone, C., and Lecomte, J. (1999) Backbone dynamics of apocytochrome b5 in its native, partially folded state. *Biochemistry 38*, 2577−2589.
73. Jin, C., and Liao, X. (1999) Backbone dynamics of a winged helix protein and its DNA complex at different temperatures: changes of internal motions in genesis upon binding to DNA. *J. Mol. Biol. 292*, 641−651.
74. Meekhof, A. E., and Freund, S. M. (1999) Probing residual structure and backbone dynamics on the milli- to picosecond time scale in a urea-denatured fibronectin type III domain. *J. Mol. Biol. 86*, 579−592.
75. Stone, M. J. (2001) NMR relaxation studies of the role of conformational entropy in stability and ligand binding. *Acc. Chem. Res. 34*, 379−388.
76. Wintrode, P. L., Zhang, D., Vaidehi, N., Arnold, F. H., and Goddard, W. A., III (2003) Protein dynamics in a family of laboratory evolved thermophilic enzymes. *J. Mol. Biol. 327*, 745−757.
77. Georgescu, R. E., Garcia-Mira, M. M., Tasayco, M. L., and Sanchez-Ruiz, J. M. (2001) Heat capacity analysis of oxidized *Escherichia coli* thioredoxin fragments (1−73, 74−108) and their noncovalent complex. Evidence for the burial of apolar surface in protein unfolded states. *Eur. J. Biochem. 268*, 1477−1485.
78. Güntert, P., Billeter, B., Ohlenschläger, O., Brown, L. R., and Wüthrich, K. (1998) Conformation analysis of protein and nucleic acid fragments with the new grid search algorithm FOUND. *J. Biomol. NMR 12*, 543−548.

BI036261D